Energy-guided combinatorial co-optimization of antibody affinity and stability

Ariel Tennenhouse[1], Adva Mechaly[2], Robert J. Oldham[3], Jake Henry[4], Isabel G. Elliott[3], Jinny Kim[3], Yael Fridmann Sirkis[5], Sveta Gaiduk[1], Daniel Christ[4], Mark S. Cragg[3], Sarel J. Fleishman[1*]

1. Department of Biomolecular Sciences, Weizmann Institute of Science, Rehovot, Israel
2. Department of Infectious Diseases, Israel Institute for Biological Research, 7410001 Ness-Ziona, Israel
3. Antibody & Vaccine Group, Centre for Cancer Immunology, School of Cancer Sciences, Faculty of Medicine, Southampton General Hospital, University of Southampton, Southampton, SO16 6YD, UK
4. Garvan Institute of Medical Research, Sydney, NSW 2010, Australia
5. Protein Analysis Unit, Weizmann Institute of Science, Rehovot, Israel
   *correspondence: sarel@weizmann.ac.il

Abstract:
Affinity maturation is an essential process in antibody engineering. Although powerful, it is iterative and time-consuming and can result in trade-offs, where affinity is gained at the cost of other essential properties, such as specificity and stability. Here, we present a scalable structure- and energy-based strategy, called LAffAb, that starts from a crystallographic structure of the bound antibody-antigen complex and introduces combinations of mutations to optimize the energy. A combinatorial mutation library comprising 7,000 variants with up to nine mutations results in large gains of up to 1,000-fold in affinity while co-optimizing antibody stability. Surprisingly, the library does not converge on a single solution; instead, it favors diverse variants with a high mutational load. Applied in small scale (10 designs) to an antibody targeting a potential drug target, designs improved affinity by an order of magnitude with little loss in specificity or stability. We envision that LAffAb can be used to select stable, specific, and high-affinity binders and to improve our understanding of sequence, structure, and function relationships in antibodies.

Main:
Molecular recognition is critical for many biological functions, with antibodies providing a prime example. Due to their tremendous versatility and compatibility with the human immune system, antibodies have been applied as therapeutics against pathological conditions ranging from cancer to neurological and autoimmune diseases and are ubiquitous reagents in all branches of biomedical research[1–3].

Binding affinity is one of several parameters that require optimization for antibodies to be effective. Among many benefits, high binding affinity can reduce dosage, nonspecific interactions, and undesirable immune reactivity[4]. Antibodies typically bind their antigens through six solvent-exposed loops called the complementarity-determining regions (CDRs). In nature, the animal immune system improves antigen-binding affinity by introducing random mutations, primarily in the CDRs, and selecting the highest-affinity variants for further randomization in an

iterative process called affinity maturation[5]. The dominant strategy for engineering improved antibody affinity emulates this natural process, routinely reaching improvements of orders of magnitude relative to those typically seen in natural antibodies[6]. Affinity maturation is, therefore, a powerful strategy; however, because finding favorable multipoint mutants in one-shot randomization is extremely unlikely, engineers must iterate mutagenesis and screening. This process is time-consuming and may result in unacceptable trade-offs in which increased affinity is attained only by compromising other properties, such as stability and specificity[7–9]. Moreover, individual mutations that improve affinity may change the backbone conformation, leading to long-range epistatic relationships between mutations in which individually favorable ones cannot be tolerated in combination[10]. Beyond these practical concerns, the fact that a critical step in developing antibodies for basic and applied biomedical research still relies on random processes reflects significant gaps in our understanding and control over antibody sequence, structure, and function.

The primary challenge for reliable design in the CDRs is their fold complexity. Antibodies often bind antigenic surfaces lacking defined secondary structure and presenting both polar and hydrophobic groups[11]. To form high-affinity and specific interactions, the CDRs must form a complementary surface that typically lacks secondary structure elements. To maintain these conformations even in the absence of the antigen, the CDRs are stabilized by an intricate network of polar and nonpolar interactions within and between the CDRs and with the framework of the antibody variable fragment (Fv)[12,13]. Given this structural complexity, design calculations must carefully weigh the potential gain from forming new interactions with the antigen against the risks of removing crucial interactions for antibody stability and foldability. An additional complication is that CDRs are extremely diverse in sequence and structure, limiting the power of statistical methods in predicting the outcome of mutations on binding.

Because of the importance of antibody affinity maturation, several computational strategies have been developed to address its limitations[14–16]. Nevertheless, because of the low likelihood of obtaining beneficial multipoint mutants, these approaches have relied on iterative mutational screening of single mutations. In one study, for instance, single-point mutations that improved electrostatic complementarity with the antigen were combined to yield 10-140 fold improvements in affinity[14]. More recently, large language models have been used to improve affinity. Here too, however, single-point mutations were experimentally screened before generating combinations[15]. In principle, AI-driven generative models may be deployed even in the absence of a bound antibody-antigen structure, but to date, they have only been successful when applied to antibodies for which large sets of mutational effects were available[15,16]. Indeed, a recent computational analysis suggested that training effective AI-driven methods for affinity prediction would require two orders of magnitude more data from accurate affinity measurements than is available in current databases[17]. Thus, because of low reliability, design methods have been restricted to iterative screening procedures[18] without addressing the main weakness that affinity maturation is a time-consuming process that may result in suboptimal solutions that compromise important properties, such as stability.

Here, we develop a non-iterative structure- and energy-based approach, called LAffAb (**L**ibraries of **Aff**ined **A**nti**b**odies), to design multipoint mutants in antibody CDRs that optimize native-state energy. To prevent loss of function due to misfolding, LAffAb starts by restricting positions that form crucial stabilizing interactions within the antibody or between the antibody and the antigen, and then searches for combinations of mutations that stabilize the antibody-antigen complex. We also developed a design approach that is compatible with high-throughput affinity screening, resulting in improvements of as much as 1,000-fold in the affinity of a model antibody. Unlike conventional computational and experimental methods, LAffAb does not iterate mutagenesis and screening and produces large and diverse sets of gain-of-function mutants. Moreover, the designs do not exhibit tradeoffs between affinity and stability, as is commonly seen in iterative selection strategies[7,9].

Results:

CDR mutation tolerance mapping

One of the main impediments to effective one-shot optimization in the CDRs is the large number of amino acid positions that form critical interactions for antibody foldability and antigen binding. We therefore start the design process with a structure- and energy-based step that maps the mutational tolerance of the CDRs (Fig. 1, step 1). Positions that make highly favorable interactions within the Fv or to the antigen are identified by computing the energy of mutations to Ala in each position of the CDRs (Fig. 1, step 2) using the Rosetta all-atom system energy (Fig. 1, step 3). Atomistic energy functions tend to penalize buried polar and electrostatic interactions due to desolvation[19], favoring hydrophobic ones in their place; however, buried polar interactions are crucial for foldability, and mutating them may lead to misfolding and dysfunction[20–22]. To mitigate this risk, we also flag positions as immutable if they contribute substantially to hydrogen-bonding energy (Fig. 1, step 4). Following these restrictions, the design workflow follows the rationale of the FuncLib approach[23], which has been successfully used to optimize obligatory and non-obligatory binding surfaces[21,24,25] and enzyme active sites[23,26]. Briefly, we exclude mutations that are rare in a multiple-sequence alignment (MSA) of antibodies in all regions except CDR H3. Because of its diversity, MSAs of H3 are unlikely to be reliable; instead, we use the per-position residue frequencies inferred by the authors of the HUCAL platinum universal antibody library[27] (Fig. 1, step 5). The remaining mutations are individually modeled in the context of the antigen-bound structure and scored in Rosetta, and mutations that substantially increase system energy are triaged (Fig. 1, step 5). Our hypothesis is that the pre-filtering steps based on atomistic calculations and observed frequencies remove mutations that destabilize the antibody or lead to backbone rearrangements, limiting the effects of long-range epistasis between mutations[10]. As an optional step, a few mutations are included in the design if visual inspection determines that they maintain or improve molecular interactions (Supp. Tables 1 and 2).

To test LAffAb, we designed a small library of variants based on the murine anti-hen egg white lysozyme (HEWL) D44.1 antibody[28], starting from a crystallographic structure of the antigen-binding fragment (Fab) bound to its antigen (PDB ID 1MLC, Fig. 1, step 1). D44.1 has served as a model system for studying affinity maturation for decades[14,24,29], allowing us to benchmark LAffAb against other approaches. Moreover, this is a high-affinity interaction (K_D of

approx. 5 nM[30,31]), and D44.1 underwent animal affinity maturation, making it representative of a typical antibody-engineering task.

Mutation tolerance mapping showed that only 18 of 59 CDR positions could be mutated without destabilizing the CDRs or the antigen-antibody complex. The majority of those (15) did not form direct interactions with the antigen (Fig. 1, step 6). D44.1, therefore, presents a case in which most CDR positions are unlikely to tolerate mutations, particularly in the most critical antigen-binding surface. Nevertheless, we hypothesized that mutations in solvent-exposed parts of the CDRs may contribute to affinity indirectly, by stabilizing the conformations of the CDRs, thus promoting the antigen-bound state as observed in the crystallographic structure.

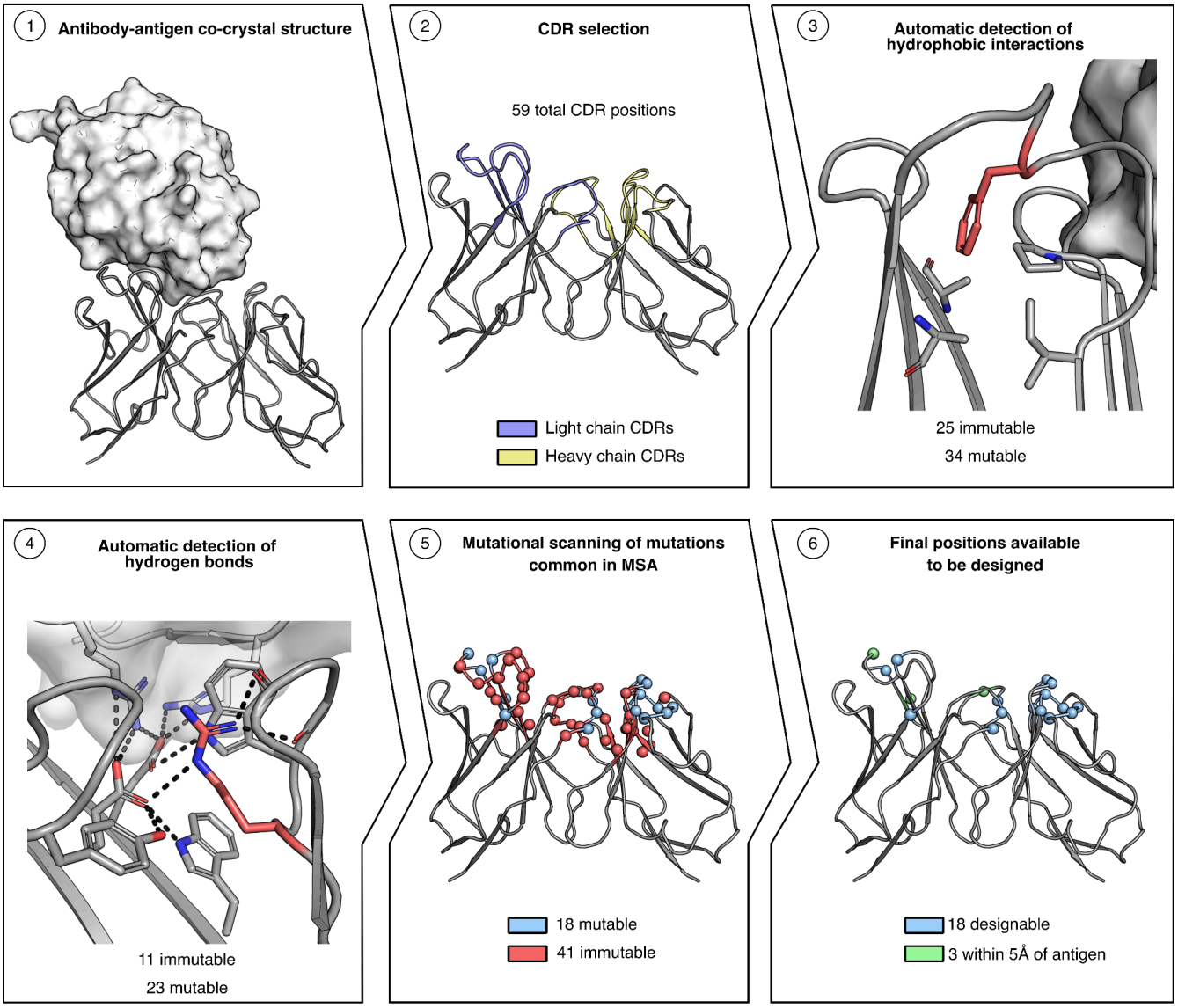

Figure 1: **Computational mutation tolerance mapping in the antibody Fv.** LAffAb begins from a co-crystal structure of an antibody-antigen complex (Step 1). CDR boundaries are automatically determined (Step 2; Supp. Table 9). Atomistic design calculations flag all positions in which mutation to Ala substantially worsens total or hydrogen-bonding energy (Steps 3 and 4, respectively). Then, mutations allowed by phylogenetic screening are modeled at each allowed CDR position, and those that substantially compromise stability are eliminated (Step 5). Mutations were mostly allowed in the periphery of the interface; only three positions in direct contact with the antigen were mutable (Step 6). Models were generated based on the co-crystal structure of D44.1 and HEWL (PDB ID 1MLC ref. [28]) using PyMOL. In steps 5 and 6, Cα atoms of indicated residues are shown as spheres.

Orders-of-magnitude affinity improvements by one-shot library design

We designed a focused combinatorial library starting from the tolerated sequence space of D44.1. The sequence space of all tolerated mutations at the 18 positions was too large to enumerate (over 1 billion mutation combinations). For computational tractability, we first removed mutations in positions far from the binding surface and ones that introduced

noncomplementary charges with the antigen (Supp. Table 1). We compared the remaining single-point mutations that comprised the designed library to those designed by a previous computational approach applied to D44.1[14]. Only two of the 17 designed point mutations mutations (Asn92$_L$Ala and Ser56$_H$Val) was shared with the previous study (Supp. Table 6). Thus, there is a small overlap between the single-point mutations designed by LAffAb and this previous approach.A significant challenge for combinatorial-library design is that mutations that are individually tolerated may be destabilizing in combination, in a phenomenon known as negative epistasis[10]. To limit this risk while also minimizing design calculations, we modelled all combinatorial mutants within each CDR separately from the other CDRs (except for L2 and H3, which are proximal and were enumerated in combination), amounting to only 115 atomistic design calculations. Each calculation modeled the combinatorial mutant and iterated sidechain packing and constrained sidechain and backbone minimization. Finally, the low-energy designs from all CDRs were combined, yielding a combinatorial library of 6,912 variants. We verified that >99% of these designs exhibited more favorable Rosetta energy than the parental antibody (Fig. 2A), suggesting that the library would be enriched for stabilized, potentially higher-affinity variants.

We assembled the designed library into single-chain variable fragments (scFv) from DNA oligos using GGAssembler[32] and screened them for binding using phage display[33]. After four rounds of panning, 22 individual colonies were sequenced. Surprisingly, we isolated 19 unique designs, and none of the isolated constructs was the parental D44.1. This suggested that despite its small size, the library comprised multiple solutions that were superior to the parent (Supp. Table 3). Furthermore, the selected designs exhibited 4-8 mutations from D44.1 (Supp. Fig. 1A), an unusually large number of mutations in single-shot affinity-maturation campaigns, verifying the reliability of the combinatorial design process. The designs were assayed for binding to HEWL using monoclonal phage ELISA, and all showed a higher binding signal than D44.1, with some exhibiting dramatic improvements (Supp. Fig. 1B).

We selected four distinct designs with 6-7 mutations from D44.1 for expression as full-length murine IgG2a antibodies (Fig. 2B). After single-step protein A purification, three exhibited purity matching or exceeding that of D44.1 (Supp. Fig. 2A, B). All four exhibited improved expression yields in Chinese hamster ovary (CHO) cells of as much as fourfold (Fig. 2C) and increases in thermal stability relative to D44.1 (Fig. 2D, Supp. Fig. 2C). Remarkably, surface plasmon resonance (SPR) experiments revealed large gains in affinity, with Des2 displaying over 1,000-fold improvement (Fig. 2E, Supp. Fig. 2D). We concluded that one-shot LAffAb calculations produced diverse variants with many CDR mutations relative to conventional single-shot antibody design and engineering processes, and that the designs exhibited large improvements in affinity together with gains in stability.

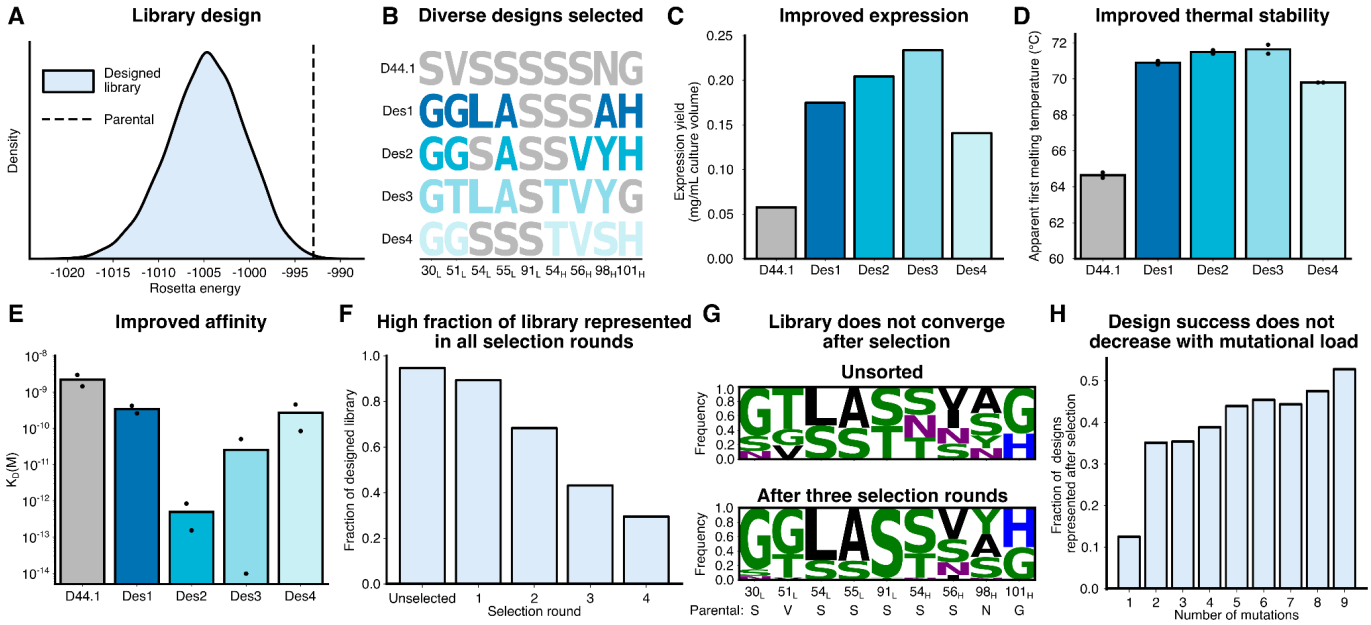

Figure 2: Design and selection of D44.1 variants that co-optimize affinity and stability. (**A**) Rosetta energy distribution of the designed library comprising 6,912 variants. Over 99% of the designed library exhibits improved Rosetta energy compared to D44.1. (**B**) Mutations at each designed position in D44.1. (**C**) Expression yield (corrected by purity) of antibodies formatted as mouse IgG2a. Based on a single measurement. (**D**) Apparent first melting temperatures measured by nano-differential scanning fluorimetry (nanoDSF). (**E**) Dissociation constants (K_D) measured by SPR. (**D, E**) Bars represent the mean of two technical replicates (measurements plotted as dots). (**F**) Fraction of the designed library present in at least one read after each phage-selection round. (**G**) Sequence logoplots of the population as a function of the selection round. Frequencies are adjusted by the number of reads for each sequence. (**H**) Fraction of the designed library observed in selection round 3. (**B, G**) Plots made with Logomaker[34].

Distinct high-affinity solutions revealed by deep sequencing

The lack of convergence in the selected binders prompted us to apply deep sequencing analysis to understand what features likely determined affinity increases. Despite the relatively small size of the library, deep sequencing showed that even after four selection rounds, 30% of the designed sequences exhibited at least one read (Fig. 2F). We used the data from the third round of selection for further analyses because the sequence of the parental D44.1 was purged by this cycle. At this selection round, most designed mutations were allowed, and some were vastly preferred relative to the parental identity (Fig. 2G, Supp. Table 4). Deep sequencing further showed that the fraction of designs with at least one read after three selection rounds showed no decrease as a function of mutational load (Fig. 2H). These results confirmed our hypothesis that the selection of tolerated point mutations according to energy and structural criteria reduces the risk of negative epistasis in combinations of individually favorable mutations. It further suggested that the space and diversity of beneficial multipoint mutants in CDRs may be very large.

Given that a large fraction of the library apparently exhibited improved affinity, we sought to understand which individual mutations failed to improve affinity. We calculated the frequency of each mutation across all designs in the selected versus unselected populations and the enrichment of each mutation in the selected population relative to that of the parental identity

(Supp. Table 4). Ten of the 16 designed single mutations had a normalized enrichment greater than 1, suggesting they were beneficial compared to the parental identity. Three others had a normalized enrichment over 0.5, suggesting they were not strongly purged. Only three mutations were strongly counter-selected: Ser91$_L$Thr, Ser54$_H$Asn, and Ser56$_H$Ile (Fig. 2G, Supp. Table 4).

Structural basis for affinity-improving mutations

We evaluated the Rosetta system energy of all single-point mutations, but they did not correlate with normalized enrichment (Supp. Fig. 3A), excluding this computed metric as a predictor. We therefore analyzed finer Rosetta energy-based filters for clues to explain the negative impact of the counter-selected mutations. Ser91$_L$Thr was in a position flagged by the computational alanine scan, because it weakens a hydrogen bond to light chain His34 (Fig. 3A, right panel). We added this deleterious mutation to test how sensitive the selection process is to conservative mutations. Structural analysis suggested that the other two deleterious mutations each introduced strain to the local backbone structure that is relieved in modeling through a subtle backbone change (0.4 and 0.6 Å between Cα atoms of the parental structure and design model of the single-point mutant; Fig. 3A, left panels). A remarkable case is presented in CDR H2 position 56. Whereas Ser56$_H$Ile is highly deleterious according to deep sequencing analysis (normalized enrichment of 0.18), a mutation to Val is allowed (0.85 normalized enrichment) and is present in Des2 (Fig. 3B left panel). A breakdown of the relative contribution to Rosetta system energy of the Val mutation suggests that this β-branched residue stabilizes the local backbone conformation (improved p_aa_pp Rosetta score[19]), but that the bulkier Ile forces an unfavorable change in the surface of HEWL (Fig. 3A, bottom left panel). Although such subtle sidechain and backbone changes may be tolerated in some contexts, due to the irregularity of the CDR conformations, such differences may elicit misfolding or compromise stability. The very large deleterious impact from adding a single methyl at the binding interface emphasizes the need for reliable atomistic design methods. By contrast, the 13 favorable or neutral mutations did not abrogate hydrogen bonds, and all mutations with enrichment better than the parental identity (Supp. Table 4) did not alter the backbone by more than 0.4 Å (Supp. Table 5, Supp. Fig. 3B). Additionally, two neighboring small-to-large mutations, Asn98$_H$Tyr, and Gly101$_H$His, may stabilize the backbone of CDR H3 by forming additional interactions with nearby positions and by reducing the desolvation penalty of the partly buried Asn in the parental D44.1 (Fig. 3B bottom right panel). Interestingly, Gly101$_H$His was not strongly favored as an individual mutation according to the deep sequencing results (Fig. 2G, Supp. Table 4), highlighting the potential of combining several weakly enhancing mutations to generate large gains in affinity.

We concluded that future applications of LAffAb should avoid mutations that are predicted to distort the local backbone structure, cause a change in the conformation of the antigen, or remove internally stabilizing hydrogen bonds. Indeed, with the benefit of hindsight, had we excluded the three deleterious mutations, the size of the library would have been reduced to 1,728 variants, of which 1,381 (80%) were observed in deep sequencing after three selection rounds.

Thus, the structural analysis suggests that combinations of stabilizing mutations, including those in the periphery of the antibody-antigen interface, can dramatically improve antibody affinity. Some mutations in the highest-affinity design are favored on their own, while others are only moderately favored or even slightly disfavored. All mutations in the highest-affinity design Des2 were not predicted by Rosetta calculations to induce substantial rearrangements of the backbone conformation nor abrogate hydrogen bonds. This analysis strongly suggests that the structure- and energy-based prefiltering of such mutations is crucial to the success of combinatorial design in CDRs. We further note that mutations that stabilize the CDRs in the periphery of the interface may be particularly attractive for design, as in most antibodies, such positions are tolerant to a greater number of mutations than interfacial ones.

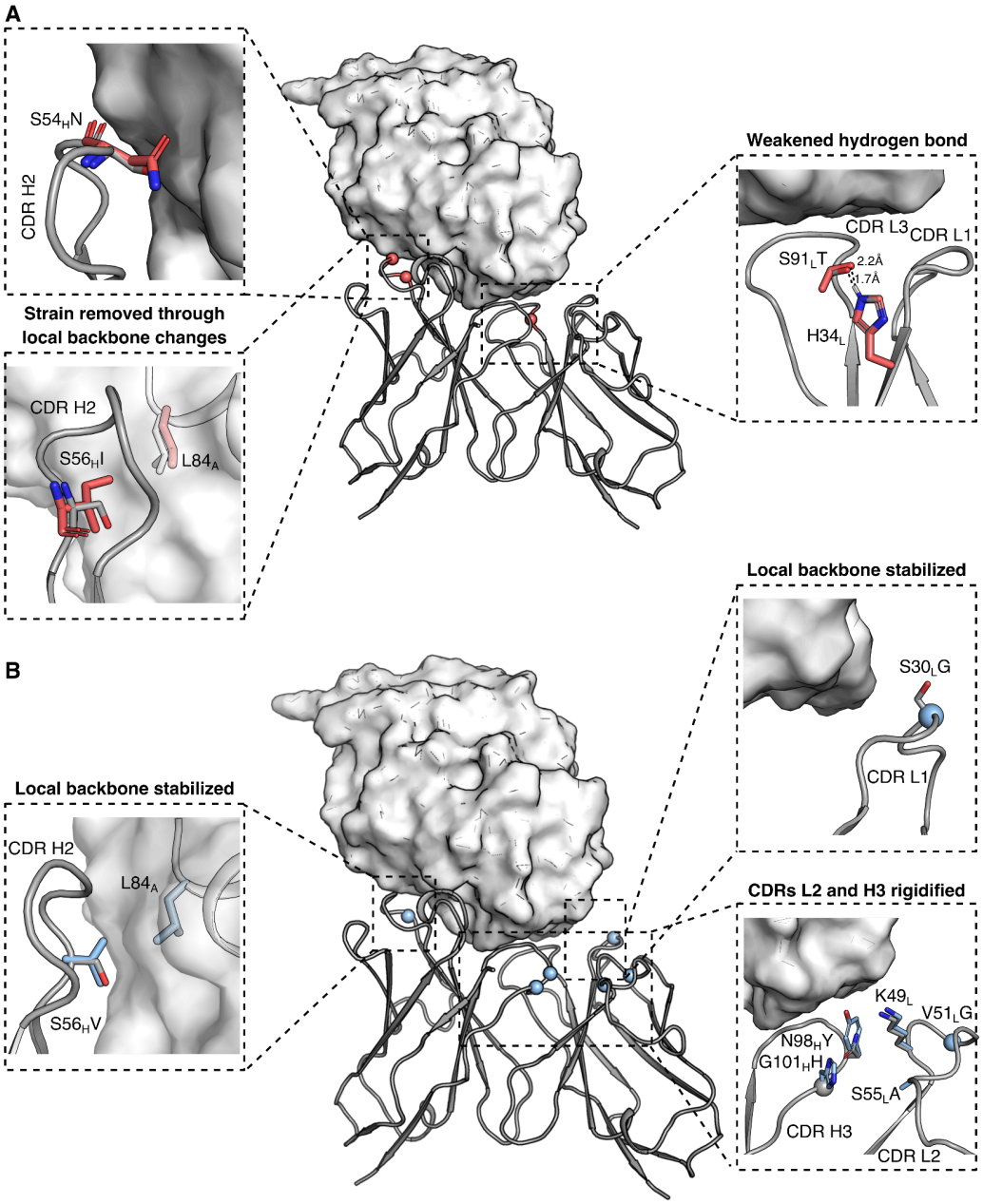

Figure 3: Structural underpinnings of favorable and deleterious mutations. (**A**) Ser91$_L$Thr (right panel) weakens a hydrogen bond with His34 in the light chain. Ser54$_H$Asn (top left panel) shifts the position of the main chain backbone atoms, potentially introducing strain into CDR H2. Similarly, Ser56$_H$Ile (bottom-left panel) changes the position of the main chain backbone atoms. Furthermore, the mutation forces a change in the conformation of Leu84 in HEWL to accommodate the larger residue. (**B**) Ser56$_H$Val likely stabilizes CDR H2 because of its β-branched side chain (left panel). A cluster of small-to-large mutations likely stabilizes CDR H3, particularly by improving interactions with Lys49 of CDR L2. (**A and B**) The middle structure shows the Rosetta-relaxed model structure of the D44.1 Fv in complex with HEWL. HEWL is shown as a surface map generated using the APBS[35] plugin in PyMOL. The Cα atoms of the mutations are shown in red (deleterious mutations) or blue (favorable) spheres in the middle panel. Inset panels show the Rosetta-relaxed model in gray and mutations in colors. Spheres in the inset panels represent glycines. Subscript L denotes light chain, subscript H denotes heavy chain, and subscript A denotes antigen (HEWL).

Large gains in affinity through low-throughput screening

Encouraged by the high fraction of improved designs in the combinatorial library, we tested whether small-scale testing of designs of an unrelated antibody-antigen complex would also lead to large affinity improvements. We applied the design process described above to the 6G08 antibody, which targets the sole inhibitory crystallizable fragment (Fc) receptor, Fc gamma Receptor IIb (FcγRIIb)[36]. FcγRIIb is expressed on both immune and non-immune cells and is engaged by the Fc of IgG in immune complexes. Its role in regulating the immune response makes it an attractive target for drug design, but antibodies against FcγRIIb can elicit opposing biological effects: antagonistic antibodies block the receptor, preventing inhibitory signalling and favoring engagement with activating FcγR, while agonistic antibodies can trigger inhibitory signalling to limit immune activation. These two opposing activities can be deployed with the potential to offer benefits in treating cancer and autoimmune disease, respectively. These opposing functions are at least in part dictated by antibody affinity[36] and Fisher et al, manuscript in preparation. Therefore, rationally designed antibodies that target FcγRIIb with altered affinity have the potential to be more effective therapeutics. However, such antibodies must also avoid binding to FcγRIIa, a key activating FcγR with 93% sequence identity to FcγRIIb in the extracellular domain as a result of segmental duplication during evolution[37] (Fig. 4A). Antibodies fulfilling these criteria were discovered using phage display, and in co-administration experiments, these increased the effectiveness of target-cell-deleting antibodies in mouse models[36]. Likely due to the harsh requirement to avoid binding to the homologous FcγRIIa during selection, the resulting affinities were low, and one specific antibody, 6G08, had particularly low affinity. 6G08, therefore, presented a stringent test of the ability of LAffAb to improve affinity without compromising specificity (Fig. 4A).

We applied the procedure described above for computational mutation tolerance mapping to the co-crystal structure of 6G08 bound to FcγRIIb[38] (PDB ID 5OCC). Unlike the D44.1-HEWL antibody, our calculations suggested many stabilizing mutations in the antibody-antigen interface of 6G08. We speculate that the reason for the difference between the two antibodies is that 6G08 had not undergone affinity maturation[36]. Because we aimed for a small set of designs rather than a combinatorial library, we enumerated all combinations of point mutations in the CDRs and selected ten designs with six mutations relative to 6G08 and 3-10 mutations relative to one another (Supp. Table 7). Some positions were flagged by the mutational tolerance mapping but were included because they improved the system and/or hydrogen-bonding energy (Supp. Table 2).

Eight of the ten designs bound FcγRIIb according to SPR. Remarkably, two of those exhibited much improved affinity of up to 30-fold (Fig. 4B, Supp. Fig. 4A). The two designs had four mutations relative to each other, suggesting that LAffAb was again able to produce distinct high-affinity solutions (Fig. 4C). Structural analysis showed that mutations in the two successful designs created new interactions with the antigen, filled cavities in the antibody-antigen interface, and stabilized the CDR backbones (Fig. 4F). To verify that the designs function in a physiological setting, they were assayed for binding to FcγRIIb-expressing CD19+ B cells within isolated peripheral blood mononuclear cells (PBMC) by flow cytometry (Fig. 4D), and both showed greatly improved binding relative to 6G08. Additionally, the designs were tested for

binding to CHO-K1 cells overexpressing the homologous off-target FcγRIIa (Fig. 4E), and both showed only weak binding, verifying that specificity was maintained. Furthermore, both designs saturated binding to FcγRIIb at 1 μg/mL, and at this concentration, both designs showed very weak binding to CHO-K1 cells overexpressing FcγRIIa, suggesting there is a significant window in which the designs can be given without detectable binding to FcγRIIa, even when FcγRIIa is overexpressed. The two designs with improved affinity maintained thermal stability (Supp. Fig. 4B, C) and >80% of the expression titer when expressed in CHO cells (Supp. Fig. 4D). Thus, 6G08 affinity for its intended target was enhanced without compromising stability or specificity with respect to a very close, evolutionarily conserved homolog of its target.

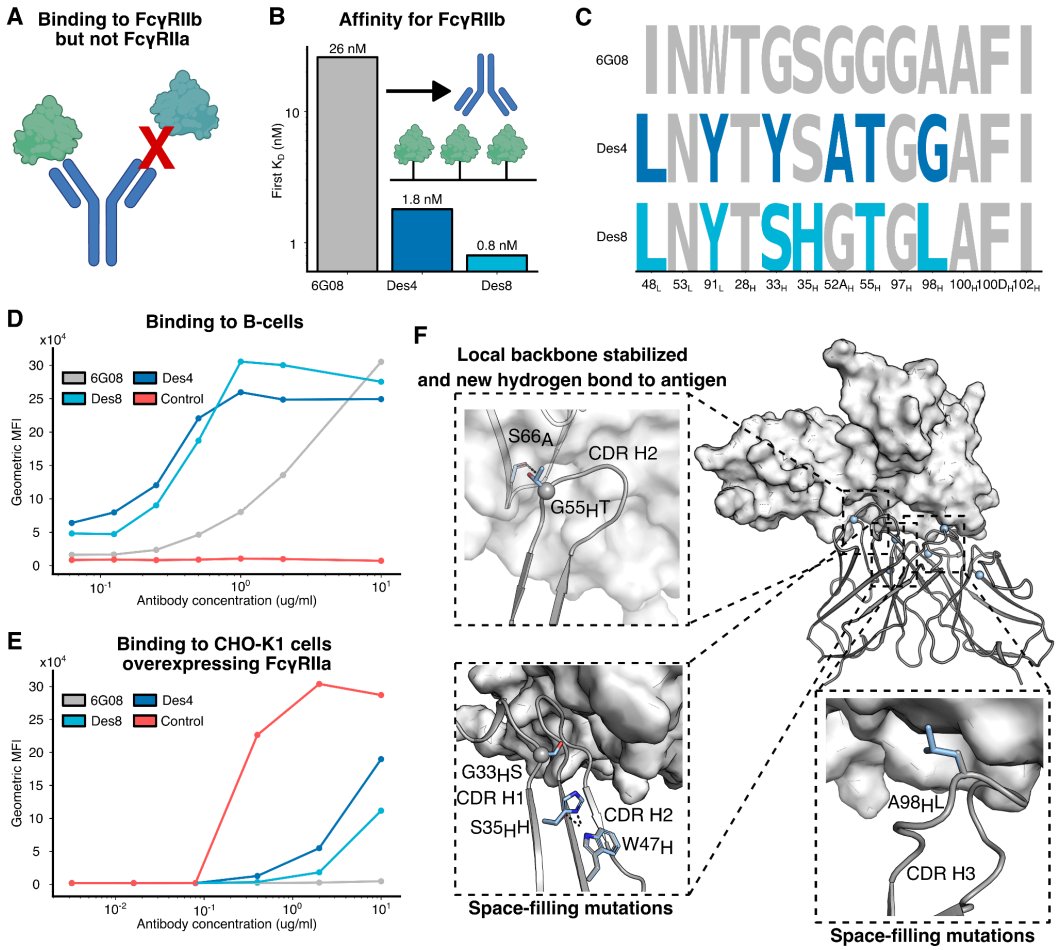

Figure 4: Improving affinity through small-scale experimental screening of antibody 6G08. (**A**) The desired outcome of the design process is high-affinity binding to FcγRIIb and not its close homolog FcγRIIa. Scheme made with BioRender. (**B**) Dissociation constants measured using SPR with FcγRIIb immobilized and antibodies flown over the chip. Inset scheme made using BioRender. Based on a single measurement. (**C**) Mutations at each designed position in 6G08 and the two successful designs. Plots made with Logomaker[34]. (**D**) Binding to B-cells isolated from PBMCs. B-cells naturally express FcγRIIb. (**E**) Binding to FcγRIIa using CHO-K1 cells overexpressing FcγRIIa. (**D and E**) Two independent experiments were performed using either directly conjugated reagents or detection with a fluorescently labelled secondary antibody. The same trend was observed in both experiments. The results using secondary detection are presented. (**F**) Structural reasoning for affinity-enhancing mutations in Des8. Gly55$_H$Thr likely stabilizes CDR H2 because of its β-branched side chain and makes a hydrogen bond with the backbone of S66 in FcγRIIb (top left panel). Two small-to-large mutations likely fill a hole in the antibody-antigen interface. Ser35$_H$H likely strengthens a hydrogen bond to Trp 47$_H$ (bottom left panel). A98$_H$L fills space in the antibody-antigen interface (right panel). The middle structure shows the Rosetta-relaxed model structure of the 6G08 Fv in complex with FcγRIIb. FcγRIIb is shown as a surface map generated using the APBS(Baker et al. 2001) plugin in PyMOL. The Cα atoms of the mutations in Des8 are shown in blue spheres in the middle panel. Inset panels show the Rosetta-relaxed model in gray and mutations in colors. Spheres in the inset panels represent glycines. Subscript L denotes light chain, subscript H denotes heavy chain, and subscript A denotes antigen (FcγRIIb).

Discussion:

A key step in the LAffAb workflow is calculating mutations that are likely to be tolerated without impacting the CDR backbone conformation. Maintaining the backbone conformation is important to enable combining multiple mutations that do not antagonize one another but is complicated by the irregularity and sensitivity of the CDRs to mutations. Thus, LAffAb is distinguished from previous natural, experimental, and computational maturation methods that prioritize single mutations without assessing their impact on the structure. Furthermore, methods that select mutations only based on their impact on affinity may inadvertently compromise stability or other desirable properties. By optimizing the energy of the antigen-bound structure subject to constraints that favor foldability, our approach, in effect, co-optimizes affinity and stability.

Our results demonstrate that positions on the CDRs may contribute to affinity, even if they do not interact directly with the antigen. This is important because interfacial positions are typically less tolerant to mutation. Surprisingly, in both test cases, we found multiple unique solutions that improve affinity, suggesting that designs could be selected to co-optimize other properties that are important in therapeutic antibodies, such as low immunogenicity and aggregation resistance[39,40].

The two case studies presented very different scenarios: in D44.1, almost no antigen-binding position was mutable, whereas in 6G08, all affinity-enhancing mutations were interfacial. Furthermore, we applied LAffAb to design 12 variants of the cetuximab antibody[41], which binds epidermal growth factor receptor (EGFR), and all designs exhibited significant decreases in binding affinity. Upon careful retrospective evaluation, we speculate that this failure resulted from abrogating an elaborate network of ordered water molecules surrounding CDR H3 (Supp. Fig. 5). The crystal structure originally used for design (PDB entry: 6ARU) did not show these water molecules while a higher resolution structure (PDB entry: 1YY9[41]) did. Our study thus highlights the need for accurate bound structures to predict mutational tolerance and how the remarkable structural diversity in antibody-antigen complexes imposes dramatically different mutational constraints.

For decades, antibody affinity optimization has been a critical step in antibody engineering that relied on iterative maturation processes[42]. LAffAb is the first approach to our knowledge that enables directly optimizing affinity and other important biophysical properties. Our study notes some important limitations to the methods applicability, including the selection of positions for design and the requirement for an accurate crystallographic structure of the antigen-bound complex. Nevertheless, the high pace of advances in antibody modeling and design methods in recent years are encouraging signs that reliable and automated methods for one-shot optimization of antibody affinity and developability may be within reach.

Methods:

Computational methods:

All Rosetta design simulations used git v.d9d4d5dd3fd516db1ad41b302d147ca0ccd78abd of the Rosetta biomolecular modeling software, which is freely available to academics at http://www.rosettacommons.org.

Selecting a set of allowed CDR mutations:

We defined the CDRs once for all antibodies in this study based on previous definitions[30,43,44] and visual inspection. CDR definitions can be found in Supp. Table 4. For each antibody, a position-specific scoring matrix (PSSM) was computed as described previously[45] for the light and heavy chain variable regions separately. Mutations were allowed at each CDR position outside of CDR H3 if they had a PSSM score >= -2. Within CDR H3, mutations were allowed from position 95-100 if they appear in human CDR H3s at a given position >=4% of the time based on per-position residue frequency data[27]. All mutations were allowed in positions 101 and 102.

As a first step, the antibody Fv structure in complex with the antigen was relaxed through cycles of sidechain and harmonically restrained backbone minimization and combinatorial sidechain packing in the entire Fv (see xmls/Relax.xml at https://github.com/Fleishman-Lab/LAffAb_public). Each CDR position was then mutated to alanine and scored using the REF15[19] score function (see xmls/alascan.xml at https://github.com/Fleishman-Lab/LAffAb_public) and the REF15 score function with the weights of all terms not related to hydrogen bonding set to zero (see xmls/alascan_Hbond.xml at https://github.com/Fleishman-Lab/LAffAb_public). Positions were considered designable if the mutation to alanine had $\Delta\Delta G$ <=3.5 REU above the parental using the REF15 score function and <= 0.6 REU using the hydrogen bond only score function. Each mutation allowed by the PSSM or CDR H3 residue frequency data was then individually modeled and scored in Rosetta (see xmls/filterscan.xml at https://github.com/Fleishman-Lab/LAffAb_public). Mutations were also modeled at positions flagged as making critical interactions, and individual mutations were allowed in these positions only if they maintained or improved these interactions (by visual inspection). For D44.1, only Ser91Thr in the light chain was allowed in a flagged position (Supp. Table 1). For 6G08, Trp91Tyr in the light chain, Ser35His in the heavy chain, Phe100$_D$Leu in the heavy chain, and Ile102Val in the heavy chain were allowed in flagged positions.

Selecting combinatorial CDR mutants:

Before combinatorial enumeration, completely solvent-exposed mutations, mutations far from the interface, and mutations that introduced unmatched charges were removed. (Supp. Tables 1 and 2). For D44.1, all combinations of allowed mutations within each CDR were enumerated. CDR L2 and CDR H3 were enumerated together because of their structural proximity. Each mutant was modeled in Rosetta, including combinatorial sidechain packing, and the backbone and sidechains of all residues were minimized, subject to harmonic restraints on the Cα

coordinates of the entire protein (see xmls/combinatorial_enumeration.xml at https://github.com/Fleishman-Lab/LAffAb_public). Each design was labeled as positive if the all-atom energy is more favorable than that of the parental antibody and negative otherwise. Mutations were removed if the variant for that mutation had $\Delta\Delta G > 1$ REU. An EpiNNet[46,47] neural network model was then trained to predict which designs are more stable than the parental antibody-antigen complex for each CDR (or CDRL2 and CDRH3 together). In short, a multi-layer perceptron classifier with a single hidden layer the size of the number of selected positions was trained on all the data. Each classifier was trained on a one-hot encoded representation of the sequence data to classify whether a sequence is more or less stable than the parental antibody. Each classifier was trained up to 20,000 iterations. Next, the single-point mutations were ranked according to their activations. Mutations are selected for the library by iteratively adding the top-ranked mutations until the fraction of sequences more stable than the parental antibody-antigen complex significantly drops. All combinations of the selected mutations for each CDR were then enumerated. Each mutant was modeled in Rosetta following the same procedure.

For 6G08, all combinations of allowed mutations within the entire Fv were enumerated. Each mutant was modeled in Rosetta, including combinatorial sidechain packing, and the backbone and sidechains of all residues were minimized, subject to harmonic restraints on the Cα coordinates of the entire protein (see xmls/combinatorial_enumeration.xml at https://github.com/Fleishman-Lab/LAffAb_public). The designs were ranked by all-atom energy. Only designs with fewer than seven mutations were considered. Positions in the antibody-antigen interface were defined using the InterfaceByVector Residue Selector in Rosetta on the antibody-antigen crystal structure (see xmls/interface.xml at https://github.com/Fleishman-Lab/LAffAb_public). Asn53 in the light chain and Gly50 in the heavy chain were manually removed from the description of the interface despite being included in the positions selected by InterfaceByVector. Designs were clustered so that each design had at least three interface mutations from all other designs, and the top ten clustered designs ranked by total score were selected.

<u>Analysis of Nanopore sequencing:</u>

The pod5 files output from nanopore were basecalled using the Dorado duplex base caller using the super accurate basecalling model. The resulting basecalled reads were then filtered to remove simplex reads already accounted for as duplex reads using SAMtools view [48]. The filtered reads were then demultiplexed using Dorado demux, and the adaptors were trimmed using Dorado trim.

Each read was aligned to a FASTA sequence of each of the constant segments between designed variable regions (6 constant segments total) using MiniMap2[49] with a minimizer kmer length of 21 (-k 21) and a minimizer window size of 11 (-w 11). The alignments were filtered to exclude unmapped reads and non-primary alignments using SAMtools view [48] (-F 3844). PySam[48] was used to iterate through the alignments for each database and filter the reads based on several properties. The query for each alignment needed to be >= 850 base pairs and <= 900 base pairs to be considered. Additionally, the query for each alignment needed to have

an average PhRed[50] score >= 20. Each alignment needed to be less than five base pairs shorter than the length of each constant segment and less than five base pairs longer than the length of each constant segment. The designed variable segments of each read were extracted based on the positions of the corresponding constant segments from the alignments. Variable segments with a high probability (>= 0.9) of having no errors based on the per-base pair PhRed scores were searched against a database of the designed variable segments, and reads with a perfect match to each designed variable segment were considered.

Antibody numbering:
Antibody numbering was performed using the AbNum[51] web server (http://www.bioinf.org.uk/abs/abnum/). Kabat numbering[43] is used throughout the work.

Distance calculations:
Distance calculations were performed using PyMOL v2.3.5.

Data visualization:
Visualization of protein structures was done using PyMOL v3.1.0. Protein surface maps were generated using the APBS[35] plug-in in PyMOL. Data visualization was done using matplotlib v3.1.0 and seaborn v0.9.0. Data was organized using pandas v0.24.2. Logo plots were made using Logomaker[34].

Experimental methods:

Assembly of DNA encoding for the D44.1 library:
GGAssembler[32] was used to optimize a set of Golden-Gate[52] overhangs to minimize the total cost of ordered oligos required to cover all mutations in the library without introducing unwanted mutations. This resulted in several variable and constant segments, with and without mutations. A gene encoding the D44.1 sequence formatted as a single-chain variable fragment was ordered from Twist BioScience. Constant segments were PCR-amplified from the gene with primers adding *BsaI* recognition sites. These and all other DNA fragments were purified using the Monarch® Spin PCR & DNA Cleanup Kit (NEB). Variable segments were ordered as single-stranded degenerate oligos from IDT. The single-stranded oligos were double-stranded by a short PCR with a single primer and purified (Roche, KAPA HiFi HotStart ReadyMix). The concentration of each segment was measured using NanoDrop One (Thermo Scientific), and TapeStation was used to assess the purity and size of each segment. A Golden-Gate assembly was conducted using the manufacturer's specifications for the light and heavy chains separately. Briefly, all segments are added at an equal amount, without the vector, and assembled using T4-ligase and BsaI-HF-v2 using cycles of 16°C and 37°C (New-England Biolabs, M202 and R3733, respectively). The resulting assemblies were PCR amplified (KAPA HiFi HotStart ReadyMix) and then combined using overlap-extension PCR, which also added the linker connecting the heavy and light chains. The final product was used to construct a phage-display library as described previously[53]. Briefly, the scFv fragments and library plasmid[54] were digested with *NcoI* and *NotI* restriction enzymes (NEB) and ligated with T4 DNA ligase

(NEB). Transformation of the desalted ligation into *E. coli* TG1 electro-competent cells (Lucigen, USA), led to $4x10^7$ transformants, greater than 1,000-fold coverage of the 7,000 variant library.

Phage display selections of the D44.1 library against HEWL:

Panning of the phage display library against plate-coated HEWL (3 µg/ml, Sigma 62970) was carried out as described[53]. Four panning cycles were performed. The buffer was alternated between each cycle between 2% skim milk and 2% Bovine serum albumin in PBS with 0.05% Tween 20. The number of input phage at each cycle decreased ($1x10^{11}$ for the first cycle, $5x10^{10}$ for the second cycle, and $1x10^{10}$ for the third and fourth cycles), and the number of washes increased with each cycle (from three in the first cycle to six for the fourth cycle). In an attempt to improve the Koff of the resultant antibodies, a parallel panning regime was carried out from the second panning cycle onward, where the last wash of the bound phages in each cycle was elongated (30, 60 and 120 minutes for the second, third and fourth cycles, respectively) and soluble HEWL (1, 1.5 and 2µM) was added.

Monoclonal phage ELISA:

Direct ELISA was performed as described previously[55]. In short, HEWL (Sigma 62970) was used to coat (3 µg/ml) maxisorb microtiter plates (Nunc, Sigma-Aldrich, St. Louis, MO, USA). Equilibrated, titrated phage were added to the blocked plate, washed, and bound phage were detected with HRP-conjugated anti-M13 antibody (Sino Biological, USA, Cat# 11973) followed by TMB substrate (Millipore, USA).

Production of anti-HEWL antibodies:

The anti-HEWL antibodies were produced by GenScript. The amino acid sequences for the light and heavy chains of D44.1 and the four designs were back-translated into DNA and codon optimized for expression in CHO cells using GeneSmart. The DNA was synthesized and cloned into an optimized murine IgG2a expression vector for the light and heavy chains separately. The plasmids were maxiprepped to yield transfection-grade plasmids using GenScript Proprietary in-house columns and reagents. The plasmids were then transiently co-transfected at a 1:1 ratio into suspension CHO-Express cell cultures. Briefly, suspension CHO cells were grown in serum-free expression medium containing GenScript proprietary in-house buffers and supplements in Erlenmeyer Flasks at 37°C with 5% CO2 on an orbital shaker. One day before transfection, the cells were seeded at 3-6x10^6 cells/mL in an Erlenmeyer flask. On the day of transfection, DNA and transfection reagent were mixed at an optimal ratio and then added to the flask with cells ready for transfection. The cell culture supernatants were collected by centrifugation at 3,000 rpm for 30 min when the cell viability was less than 50%. The supernatants were loaded onto AmMag Protein A Magnetic Beads (GenScript cat L00695) and incubated for the appropriate time. The beads were washed and eluted using GenScript Proprietary in-house columns and reagents. The eluted fractions were pooled and buffer exchanged to 1X PBS pH 7.2. The purified protein was analyzed by SDS-PAGE analysis using a 4%~20% gradient SDS-PAGE gel (GenScript Cat.No. M42012) to determine the molecular weight and purity. Each sample was run in reducing sample buffer (60 mM Tris-HCl, 2% SDS, 6% Glycerol, 0.1% bromophenol blue, 50 mM DTT, pH 6.8) and non-reducing sample buffer (50 mM Tris-HCl, 1% SDS, 6% Glycerol, 0.1% bromophenol blue, 50 mM NEM, pH 6.8). The

endotoxin level of protein was also detected using a Kinetic Turbidimetric Assay (Bioendo). The concentration was determined by measuring A280 using a NanoDrop Ultra (ThermoScientific). The final yield was calculated by multiplying the concentration by the total volume of the eluate. The final yield was then corrected by the purity measured using SDS-PAGE.

NanoDSF of anti-HEWL antibodies:

The first apparent melting temperature of the antibodies was determined using the Prometheus Panta instrument (NanoTemper). Full-length antibodies formatted as IgG2a were diluted to 0.2 mg/mL in 1X PBS. The temperature was ramped from 20 °C to 100 °C at 1.0 °C per minute. The first apparent melting temperatures were identified using the Prometheus Panta software (v. 1.4.4) with default parameters.

SPR of anti-HEWL antibodies:

SPR experiments on the anti-HEWL antibodies were carried out on a Biacore 8K instrument (Cytiva) at 25 °C with PBST (1X PBS + 0.05% Tween-20). For binding analysis, each antibody was immobilized to a flow cell of a protein A sensor chip (Cytiva 29127555) at a concentration of 5 µg/mL (corrected by purity from SDS-PAGE) in 1X PBS for 60 sec at a flow rate of 10 µL/min. A reference flow cell for each channel was not loaded with antibody. Approximately 100-200 response units of each antibody were immobilized. Samples of different HEWL (Sigma 62970) concentrations (1.25, 0.63, 0.31, 0.16, and 0.08 nM) were injected over the surface at a flow rate of 30 µL/min for 240 s, and the chip was washed with PBST for 600 sec at a flow rate of 30 µL/min. After each injection, surface regeneration was performed with a 30-second injection of 10 mM glycine pH 1.5 at a flow rate of 10 µL/min, and reached the same baseline. The sensogram for each flow cell without antibody was subtracted from the sensogram for the flow cell with antibody from the same channel. The acquired sensograms were analysed using the device's software (v.4.0.8.19879), and kinetic fits to a 1:1 binding model were performed with global fitting of kon, koff, Rmax, and tc with standard initial values. RI was fit to a constant of 0, and drift was fit locally with an initial value of 0. The experiment was repeated using different samples of HEWL and different dilutions of the antibodies.

Production of anti-FcγRIIb antibodies:

The variable heavy and light chain sequences of the antibodies were cloned into pEE6.4 expression vectors (Lonza) containing human IgG1 constant domains. Plasmid DNA was prepared using a DNA miniprep kit (Qiagen), and constructs were verified by Sanger sequencing (Source BioScience). ExpiCHO cells (Thermo Fisher) were cultured at 37°C with 8% CO2 and shaking at 125 rpm. Transient transfections were performed at a density of 6.0 X 10^6 cells/ml following the manufacturer's protocol, and cultures were harvested 7 days post-transfection. Antibodies were purified using a Protein A MabSelect SuRe column (Cytiva) on an AKTA Start chromatography system. Purity and integrity were confirmed by gel electrophoresis and HPLC, and endotoxin levels were measured for downstream applications.

SPR of anti-FcγRIIb antibodies:

SPR was performed using a Biacore T100 upgraded to T200 sensitivity (Cytiva). An anti-HIS antibody was immobilised on a Biacore CM5 chip. Recombinant human FcγRIIb (R&D Systems)

at 0.5µg/ml was captured with a target of 100 RU. Antibodies at indicated concentrations were then flowed at 30 µL/ml for 4 minutes, followed by a 5-minute dissociation with HBS-EP+ (Cytiva) used as running buffer. Data was analysed using Biacore Evaluation software and fitted to a bivalent model.

Flow cytometry staining of B-cells:

Leukocyte cones were obtained from healthy donors from the Southampton NHS Blood and Transplant Service. Use was approved by the University of Southampton Faculty of Medicine Ethics Committee and East of Scotland Research Ethics Service, Research ethical committee reference number 16/ES/0048. PBMC were isolated using lymphoprep (Stemcell Technologies). $2.5x10^5$ PBMC were stained with 1µl anti-CD19 PE-Cy7 (Biolegend) and 6G08 antibodies at the indicated concentrations for 30 minutes at 4°C. Cells were washed, and 0.5 µl PE goat anti-human IgG (Jackson Immunoresearch) was added for 30 minutes at 4°C. After washing, samples were run on a Cytoflex flow cytometer (Beckman Coulter). Data was analysed using FlowJo v10 (BD Biosciences) by gating on single cells, identifying lymphocytes based on FSC vs. SSC, and gating on CD19+ B cells.

Flow cytometry staining of CHO-K1 cells overexpressing FcγRIIa:

CHO-K1 cells stably expressing hFcγRIIa (H131) were generated as described previously[56] and were maintained in RPMI + 10% FCS (Sigma-Aldrich), glutamine (2mM), sodium pyruvate (1mM), penicillin (100 U/ml), streptomycin (100 ug/ml) and 10 ug/ml puromycin (invivogen), all Life Technologies unless otherwise stated. Cells were stained with 6G08 antibodies as above, washed, and run on a Cytoflex flow cytometer (Beckman Coulter).

nano-DSF of anti-FcγRIIb antibodies:

Thermal stability of antibodies was assessed by nano differential scanning fluorimetry (nanoDSF) using the Prometheus NT.48 (NanoTemper Technologies, Munich, Germany). Samples were loaded into Prometheus standard capillaries at approximately 1 mg/mL and exposed to thermal stress from 15°C to 95°C, with a ramp of 1°C/min. Intrinsic protein fluorescence was measured at 330 nm and 350 nm. Melting temperature (Tm) was calculated by PR.ThermControl software (NanoTemper Technologies) using first derivative analysis of the 350/330 nm fluorescence ratio plotted against temperature.

Contributions:

A.T. and S.J.F. conceived the idea. A.T. and S.J.F. wrote the paper, with input from all authors. A.T. developed the affinity optimization algorithm and designed all amino acid sequences. A.M. assembled the anti-HEWL library and performed the phage display screening. A.T. performed biophysical characterization of anti-HEWL antibodies with the help of Y.F.S.. S.G. prepared the anti-HEWL sequences for deep sequencing. A.T. performed the deep sequencing experiment, and A.T. and S.J.F. analyzed the data. R.J.O., I.G.E., and J.K. performed experimental work related to the anti-FcγRIIb antibodies, and A.T., S.J.F., R.O., I.G.E., and M.S.C. analyzed the data. J.H. performed the experimental work related to Cetuximab, and J.H., D.C., A.T., and S.J.F. analyzed the data. S.J.F., M.S.C., and D.C. were responsible for funding acquisition.

Acknowledgments:
We thank the Membrane Protein Laboratory at the Diamond Light Source for access to the Prometheus NT.48 instrument. The Membrane Protein Laboratory is funded by a grant from the Wellcome Trust (223727/Z/21/Z) with additional support provided by Diamond Light Source and the Research Complex at Harwell, both Instruct-ERIC centers. We thank Dina Listov (Weizmann Institute of Science), Olga Khersonsky (Weizmann Institute of Science), Rebecca Wilen (Weizmann Institute of Science), Mimi Schwartz (Weizmann Institute of Science), Ahuva Nissim (Queen Mary University of London and Weizmann Institute of Science), and Hayden Fisher (ESRF) for critical discussions on the work. A.T. was supported by Teva Pharmaceutical Industries Ltd as part of the Israeli National Forum for BioInnovators (NFBI) and by the Azrieli Foundation under the Azrieli Fellows Program. I.G.E. and M.S.C. were supported by a grant from Cancer Research UK, DRCPGM\100039. The study was supported by a European Research Council Advanced Grant (101140394) to S.J.F.

Competing interests:
M.S.C. acts as a retained consultant for BioInvent International, consults for several other biotech companies, and receives institutional payments and royalties from antibody licenses. He has received research funding from BioInvent, GSK, iTeos, UCB, Surrozen, and Roche. S.J.F. and A.T. are named inventors on patents related to antibody design. S.J.F. is a paid advisor on protein design.

Data availability:
Amino acid sequences of the Fvs of the four anti-HEWL and ten anti-FcγRIIb designed variants characterized as IgG are available in Supp. Tables 10 and 11. The anti-HEWL deep sequencing data will be made available upon publication.

References:

1. Strohl, W. R. Structure and function of therapeutic antibodies approved by the US FDA in 2024. *Antib. Ther.* (2025) doi:10.1093/abt/tbaf014.
2. Bradbury, A. & Plückthun, A. Reproducibility: Standardize antibodies used in research. *Nature* **518**, 27–29 (2015).
3. Chan, A. C., Martyn, G. D. & Carter, P. J. Fifty years of monoclonals: the past, present and future of antibody therapeutics. *Nat. Rev. Immunol.* (2025) doi:10.1038/s41577-025-01207-9.
4. Lu, R.-M. *et al.* Development of therapeutic antibodies for the treatment of diseases. *J. Biomed. Sci.* **27**, 1 (2020).
5. Victora, G. D. & Nussenzweig, M. C. Germinal centers. *Annu. Rev. Immunol.* **30**, 429–457 (2012).
6. Hu, D. *et al.* Effective optimization of antibody affinity by phage display integrated with high-throughput DNA synthesis and sequencing technologies. *PLoS One* **10**, e0129125 (2015).
7. Julian, M. C., Li, L., Garde, S., Wilen, R. & Tessier, P. M. Efficient affinity maturation of antibody variable domains requires co-selection of compensatory mutations to maintain thermodynamic stability. *Sci. Rep.* **7**, (2017).
8. Shehata, L. *et al.* Affinity maturation enhances antibody specificity but compromises conformational stability. *Cell Rep.* **28**, 3300–3308.e4 (2019).
9. Rabia, L. A., Desai, A. A., Jhajj, H. S. & Tessier, P. M. Understanding and overcoming trade-offs between antibody affinity, specificity, stability and solubility. *Biochem. Eng. J.* **137**, 365–374 (2018).
10. Lipsh-Sokolik, R. & Fleishman, S. J. Addressing epistasis in the design of protein function. *Proc. Natl. Acad. Sci. U. S. A.* **121**, e2314999121 (2024).
11. Zhou, J., Le, C. Q., Zhang, Y. & Wells, J. A. A general approach for selection of epitope-directed binders to proteins. *Proc. Natl. Acad. Sci. U. S. A.* **121**, e2317307121 (2024).
12. Foote, J. & Winter, G. Antibody framework residues affecting the conformation of the hypervariable loops. *J. Mol. Biol.* **224**, 487–499 (1992).
13. Makabe, K. *et al.* Thermodynamic consequences of mutations in vernier zone residues of a humanized anti-human epidermal growth factor receptor murine antibody, 528. *J. Biol. Chem.* **283**, 1156–1166 (2008).
14. Lippow, S. M., Wittrup, K. D. & Tidor, B. Computational design of antibody-affinity improvement beyond in vivo maturation. *Nat. Biotechnol.* **25**, 1171–1176 (2007).
15. Hie, B. L. *et al.* Efficient evolution of human antibodies from general protein language models. *Nat. Biotechnol.* **42**, 275–283 (2024).
16. Shanker, V. R., Bruun, T. U. J., Hie, B. L. & Kim, P. S. Unsupervised evolution of protein and antibody complexes with a structure-informed language model. *Science* **385**, 46–53 (2024).
17. Hummer, A. M., Schneider, C., Chinery, L. & Deane, C. M. Investigating the volume and diversity of data needed for generalizable antibody-antigen ΔΔG prediction. *Nat. Comput. Sci.* **5**, 635–647 (2025).
18. Frey, N. C. *et al.* Lab-in-the-loop therapeutic antibody design with deep learning. *bioRxiv* (2025) doi:10.1101/2025.02.19.639050.
19. Alford, R. F. *et al.* The Rosetta all-atom energy function for macromolecular modeling and design. *J. Chem. Theory Comput.* **13**, 3031–3048 (2017).
20. Baran, D. *et al.* Principles for computational design of binding antibodies. *Proc. Natl. Acad. Sci. U. S. A.* **114**, 10900–10905 (2017).
21. Netzer, R. *et al.* Ultrahigh specificity in a network of computationally designed protein-interaction pairs. *Nat. Commun.* **9**, 5286 (2018).

22. Khersonsky, O. & Fleishman, S. J. What Have We Learned from Design of Function in Large Proteins? *BioDesign Research* **2022**, 1–11 (2022).
23. Khersonsky, O. *et al.* Automated design of efficient and functionally diverse enzyme repertoires. *Mol. Cell* **72**, 178–186.e5 (2018).
24. Warszawski, S. *et al.* Optimizing antibody affinity and stability by the automated design of the variable light-heavy chain interfaces. *PLoS Comput. Biol.* **15**, e1007207 (2019).
25. VanDrisse, C. M., Lipsh-Sokolik, R., Khersonsky, O., Fleishman, S. J. & Newman, D. K. Computationally designed pyocyanin demethylase acts synergistically with tobramycin to kill recalcitrant Pseudomonas aeruginosa biofilms. *Proc. Natl. Acad. Sci. U. S. A.* **118**, (2021).
26. Listov, D. *et al.* Complete computational design of high-efficiency Kemp elimination enzymes. *Nature* **643**, 1421–1427 (2025).
27. Prassler, J. *et al.* HuCAL PLATINUM, a synthetic Fab library optimized for sequence diversity and superior performance in mammalian expression systems. *J. Mol. Biol.* **413**, 261–278 (2011).
28. Braden, B. C. *et al.* Three-dimensional structures of the free and the antigen-complexed Fab from monoclonal anti-lysozyme antibody D44.1. *J. Mol. Biol.* **243**, 767–781 (1994).
29. Cauerhff, A., Goldbaum, F. A. & Braden, B. C. Structural mechanism for affinity maturation of an anti-lysozyme antibody. *Proc. Natl. Acad. Sci. U. S. A.* **101**, 3539–3544 (2004).
30. Tennenhouse, A. *et al.* Computational optimization of antibody humanness and stability by systematic energy-based ranking. *Nat. Biomed. Eng.* **8**, 30–44 (2024).
31. Hutchinson, M. *et al.* Toward enhancement of antibody thermostability and affinity by computational design in the absence of antigen. *MAbs* **16**, 2362775 (2024).
32. Hoch, S. Y. *et al.* GGAssembler: Precise and economical design and synthesis of combinatorial mutation libraries. *Protein Sci.* **33**, e5169 (2024).
33. Winter, G., Griffiths, A. D., Hawkins, R. E. & Hoogenboom, H. R. Making antibodies by phage display technology. *Annu. Rev. Immunol.* **12**, 433–455 (1994).
34. Tareen, A. & Kinney, J. B. Logomaker: beautiful sequence logos in Python. *Bioinformatics* **36**, 2272–2274 (2020).
35. Baker, N. A., Sept, D., Joseph, S., Holst, M. J. & McCammon, J. A. Electrostatics of nanosystems: application to microtubules and the ribosome. *Proc. Natl. Acad. Sci. U. S. A.* **98**, 10037–10041 (2001).
36. Roghanian, A. *et al.* Antagonistic human FcγRIIB (CD32B) antibodies have anti-tumor activity and overcome resistance to antibody therapy in vivo. *Cancer Cell* **27**, 473–488 (2015).
37. Frampton, S. *et al.* Fc gamma receptors: Their evolution, genomic architecture, genetic variation, and impact on human disease. *Immunol. Rev.* **328**, 65–97 (2024).
38. Sutton, E. J. *et al.* Evaluating anti-CD32b F(ab) conformation using molecular dynamics and small-angle X-ray scattering. *Biophys. J.* **115**, 289–299 (2018).
39. Makowski, E. K. *et al.* Optimization of therapeutic antibodies for reduced self-association and non-specific binding via interpretable machine learning. *Nat. Biomed. Eng.* **8**, 45–56 (2024).
40. Carter, P. J. & Quarmby, V. Immunogenicity risk assessment and mitigation for engineered antibody and protein therapeutics. *Nat. Rev. Drug Discov.* **23**, 898–913 (2024).
41. Li, S. *et al.* Structural basis for inhibition of the epidermal growth factor receptor by cetuximab. *Cancer Cell* **7**, 301–311 (2005).
42. Low, N. M., Holliger, P. H. & Winter, G. Mimicking somatic hypermutation: affinity maturation of antibodies displayed on bacteriophage using a bacterial mutator strain. *J. Mol. Biol.* **260**, 359–368 (1996).
43. MacCallum, R. M., Martin, A. C. & Thornton, J. M. Antibody-antigen interactions: contact analysis and binding site topography. *J. Mol. Biol.* **262**, 732–745 (1996).

44. Dondelinger, M. *et al.* Understanding the significance and implications of antibody numbering and antigen-binding surface/residue definition. *Front. Immunol.* **9**, 2278 (2018).
45. Goldenzweig, A. *et al.* Automated structure- and sequence-based design of proteins for high bacterial expression and stability. *Mol. Cell* **70**, 380 (2018).
46. Weinstein, J. Y. *et al.* Designed active-site library reveals thousands of functional GFP variants. *Nat. Commun.* **14**, 2890 (2023).
47. Lipsh-Sokolik, R. *et al.* Combinatorial assembly and design of enzymes. *Science* **379**, 195–201 (2023).
48. Li, H. *et al.* The Sequence Alignment/Map format and SAMtools. *Bioinformatics* **25**, 2078–2079 (2009).
49. Li, H. Minimap2: pairwise alignment for nucleotide sequences. *Bioinformatics* **34**, 3094–3100 (2018).
50. Ewing, B., Hillier, L., Wendl, M. C. & Green, P. Base-calling of automated sequencer traces using phred. I. Accuracy assessment. *Genome Res.* **8**, 175–185 (1998).
51. Abhinandan, K. R. & Martin, A. C. R. Analysis and improvements to Kabat and structurally correct numbering of antibody variable domains. *Mol. Immunol.* **45**, 3832–3839 (2008).
52. Engler, C., Kandzia, R. & Marillonnet, S. A one pot, one step, precision cloning method with high throughput capability. *PLoS One* **3**, e3647 (2008).
53. Noy-Porat, T. *et al.* A panel of human neutralizing mAbs targeting SARS-CoV-2 spike at multiple epitopes. *Nat. Commun.* **11**, 4303 (2020).
54. Azriel-Rosenfeld, R., Valensi, M. & Benhar, I. A human synthetic combinatorial library of arrayable single-chain antibodies based on shuffling in vivo formed CDRs into general framework regions. *J. Mol. Biol.* **335**, 177–192 (2004).
55. Mechaly, A. *et al.* Novel phage display-derived anti-abrin antibodies confer post-exposure protection against abrin intoxication. *Toxins (Basel)* **10**, 80 (2018).
56. Tutt, A. L. *et al.* Development and characterization of monoclonal antibodies specific for mouse and human fcγ receptors. *J. Immunol.* **195**, 5503–5516 (2015).